NeuroImage 103 (2014) 171–180

Contents lists available at ScienceDirect

NeuroImage

journal homepage: www.elsevier.com/locate/ynimg

SPECT-imaging of activity-dependent changes in regional cerebral blood flow induced by electrical and optogenetic self-stimulation in mice

Angela Kolodziej [a,b,1], Michael Lippert [a,1], Frank Angenstein [c], Jenni Neubert [a], Annette Pethe [d], Oliver S. Grosser [d], Holger Amthauer [d], Ulrich H. Schroeder [a], Klaus G. Reymann [a,c], Henning Scheich [a,e], Frank W. Ohl [a,b,e], Jürgen Goldschmidt [a,f,*]

[a] Leibniz-Institute for Neurobiology, Brenneckestr. 6, D-39118 Magdeburg, Germany
[b] Otto von Guericke University Magdeburg, Institute of Biology, Leipziger Strasse 44, D-39120 Magdeburg, Germany
[c] Deutsches Zentrum für neurodegenerative Erkrankungen (DZNE), Leipziger Strasse 44, D-39120 Magdeburg, Germany
[d] Department of Radiology and Nuclear Medicine, University Hospital Magdeburg, Leipziger Strasse 44, D-39120 Magdeburg, Germany
[e] Center for Behavioral Brain Sciences (CBBS), Otto-von-Guericke-University Magdeburg, Universitätsplatz 2, D-39106 Magdeburg, Germany
[f] Otto-von-Guericke University Magdeburg, Department of Neurology, Leipziger Str. 44, D-39120 Magdeburg, Germany

ARTICLE INFO

Article history:
Accepted 8 September 2014
Available online 16 September 2014

Keywords:
SPECT
PET
fMRI
mouse
reward
optogenetics

ABSTRACT

Electrical and optogenetic methods for brain stimulation are widely used in rodents for manipulating behavior and analyzing functional connectivities in neuronal circuits. High-resolution in vivo imaging of the global, brain-wide, activation patterns induced by these stimulations has remained challenging, in particular in awake behaving mice. We here mapped brain activation patterns in awake, intracranially self-stimulating mice using a novel protocol for single-photon emission computed tomography (SPECT) imaging of regional cerebral blood flow (rCBF). Mice were implanted with either electrodes for electrical stimulation of the medial forebrain bundle (mfb-microstim) or with optical fibers for blue-light stimulation of channelrhodopsin-2 expressing neurons in the ventral tegmental area (vta-optostim). After training for self-stimulation by current or light application, respectively, mice were implanted with jugular vein catheters and intravenously injected with the flow tracer 99 m-technetium hexamethylpropyleneamine oxime (99mTc-HMPAO) during seven to ten minutes of intracranial self-stimulation or ongoing behavior without stimulation. The 99mTc-brain distributions were mapped in anesthetized animals after stimulation using multipinhole SPECT. Upon self-stimulation rCBF strongly increased at the electrode tip in mfb-microstim mice. In vta-optostim mice peak activations were found outside the stimulation site. Partly overlapping brain-wide networks of activations and deactivations were found in both groups. When testing all self-stimulating mice against all controls highly significant activations were found in the rostromedial nucleus accumbens shell. SPECT-imaging of rCBF using intravenous tracer-injection during ongoing behavior is a new tool for imaging regional brain activation patterns in awake behaving rodents providing higher spatial and temporal resolutions than 18 F-2-fluoro-2-dexoyglucose positron emission tomography.

Introduction

Techniques for artificial stimulation of brain circuits are increasingly used for manipulating behavior and analyzing functional connectivities in the brains of laboratory animals. Mapping the brain-wide effects of such stimulations is crucial for understanding the link between behavioral output and activated circuits. This is of special relevance in mice, where a broad range of tools has become available for optogenetic stimulations (Boyden et al., 2005; Yizhar et al., 2011). Given the increasing number of such studies methods that can image animals at high throughput will be of particular interest.

The effects of stimulations can be mapped at high spatial resolution using histochemical techniques like 2-deoxyglucose autoradiography (Porrino et al., 1984), c-fos immunocytochemistry (Thanos et al.,

* Corresponding author at: Leibniz-Institute for Neurobiology, Department Systems Physiology of Learning, Brenneckestr. 6, D-39118 Magdeburg, Germany.
E-mail addresses: angela.kolodziej@lin-magdeburg.de (A. Kolodziej), mlippert@lin-magdeburg.de (M. Lippert), frank.angenstein@dzne.de (F. Angenstein), jenni.neubert@charite.de (J. Neubert), annette.pethe@med.ovgu.de (A. Pethe), oliver.grosser@med.ovgu.de (O.S. Grosser), holger.amthauer@med.ovgu.de (H. Amthauer), ulrich.schroeder@lin-magdeburg.de (U.H. Schroeder), reymann@lin-magdeburg.de (K.G. Reymann), henning.scheich@lin-magdeburg.de (H. Scheich), frank.ohl@lin-magdeburg.de (F.W. Ohl), juergen.goldschmidt@lin-magdeburg.de (J. Goldschmidt).
[1] These authors contributed equally to this work.

http://dx.doi.org/10.1016/j.neuroimage.2014.09.023
1053-8119/

2013) or thallium autometallography (Goldschmidt et al., 2010). Data acquisition and data analysis, however, are time-consuming using these methods. In vivo imaging techniques based on magnetic resonance imaging (MRI), positron emission tomography (PET) or single-photon emission computed tomography (SPECT) are better suited to screen for whole-brain activation patterns in the rodent brain as they provide more rapid access to quantitative three-dimensional data sets and enable repeated imaging of the same animals.

The most widely used approach for in vivo imaging of the effects of electrical or optogenetic stimulations in rodents is BOLD-fMRI (Angenstein et al., 2009; Lee et al., 2010; Desai et al., 2011; Kahn et al., 2011; Abe et al., 2012.) This method, however, requires the animals to be anesthetized or restrained inside scanners severely limiting the range of behavioral paradigms that can be studied. Effects of stimulations in awake unrestrained rats can be mapped using ^{18} F-2-fluoro-2-deoxyglucose PET (^{18} F-FDG-PET) (Thanos et al., 2013), but with typical spatial resolutions in the 1–2 mm range ^{18} F-FDG-PET has remained less attractive for studying spatial patterns of neuronal activity in mice.

We here introduce SPECT-imaging of regional cerebral blood flow (rCBF) for mapping the effects of electrical and optical stimulation in awake behaving mice.

SPECT has long been regarded as an imaging technique with low spatial resolution. During the past decade, however, based on pinhole collimation (Beekman and van der Have, 2007) small-animal SPECT-scanners have been developed that outperform micro-PET scanners in terms of spatial resolution. Using the blood flow tracer 99 m-technetium hexamethylpropyleneamine-oxime (^{99m}Tc-HMPAO) spatial patterns of neuronal activity can be mapped in the rodent brain (Wyckhuys et al., 2010, 2013).

The lipophilic flow tracer ^{99m}Tc-HMPAO has been used for decades for imaging rCBF in humans (McArthur et al., 2011; Neirinckx et al., 1987). After crossing the blood–brain barrier the tracer is rapidly converted to a hydrophilic compound that remains trapped in the brain and shows no redistribution. Similar in rationale to ^{18} F-FDG-PET, ^{99m}Tc-HMPAO-SPECT can, in principle, be used for imaging brain activation patterns in awake behaving rodents. Both tracers can be injected in the awake state and the stable brain tracer-distributions after stimulation can be mapped in the anesthetized state. Thus far, however, ^{99m}Tc-HMPAO-SPECT has only been used in restrained rats (Wyckhuys et al., 2010, 2013) or anesthetized mice (Apostolova et al., 2012).

We here used ^{99m}Tc-HMPAO-SPECT for imaging activity-dependent changes in rCBF in intracranially self-stimulating mice. We implanted mice with either electrodes for electrical stimulation of the medial forebrain bundle (mfb) or with fibers for optical stimulation of channelrhodopsin-2 expressing neurons in the ventral tegmental area (VTA). Mice were trained for self-stimulation by current or light application, respectively. After training we implanted mice with jugular vein catheters and intravenously injected ^{99m}Tc-HMPAO during several minutes of ongoing intracranial self-stimulation or during control conditions without stimulation. After stimulation we mapped, in the anesthetized animals, the ^{99m}Tc-distribution. We co-registered the SPECT images with CT images and aligned the SPECT/CT data sets with anatomical MRI scans of individual mice and reference MRI images (Ma et al., 2005, 2008). Using this protocol we provide the first SPECT-images of activity-dependent changes in rCBF in mouse brain.

Materials and Methods

Animals

Adult male C57Bl6/J mice at the age of eight weeks were used in this study. Mice were obtained from Charles River (Sulzfeld, Germany) and initially housed in groups of 3 or 4 in clear, polycarbonate cages (Duracage, Siloam Springs, USA) lined with commercial animal bedding. Food pellets and tap water were freely available. Mice were maintained in a separate room with 12 h light/dark cycle (light on at 6.00 am). After one week of acclimation to the laboratory, mice were assigned to either the electrical or the optogenetic self-stimulation group. The experimental procedure of this study is illustrated in Fig. 1.

Self-stimulation mediated by electrical stimulation of the mfb

Mice were anesthetized with ketamine (200 mg/kg) (Pharmacia GmbH, Berlin, Germany) and xylazine (7 mg/kg) (Bayer, Leverkusen, Germany), fixated in a stereotaxic frame and implanted bilaterally with bipolar Teflon insulated electrodes (75 μm diameter, Science products, Hofheim, Germany) aimed at the medial forebrain bundle (mfb) at the level of the lateral hypothalamus (AP −1.0; ML ±1.0; DV −5.0) using coordinates from the Paxinos and Franklin (1997) mouse atlas. Electrodes were attached to a small plug (Molex, Dreieich, Germany) that was cemented to the skull via dental cement (RelyXTM Luting, 3 M ESPE, Seefeld, Germany). After surgery, mice were allowed to recover on a heating pad for 1 hour and were housed individually for the duration of the experiments.

After a recovery period of at least one week after electrode implantation mice were placed in a small polycarbonate box and trained to press a lever for intracranial self-stimulation via brief electrical pulses (200 ms trains, 20 biphasic pulses of 0.2 ms duration at 100Hz) generated by an isolated pulse stimulator (Model 2100, A-M Systems Inc., Carlsborg, USA). Initially, electrodes in both hemispheres were assessed. The electrode that supported more frequent lever pressing was chosen for further optimization. Mice showed robust self-stimulation behavior within 1–3 days. Subsequently, optimal stimulus intensity was determined for each animal by using ascending and descending stimulation intensities in two separate sessions (steps of 20 μA, each intensity was used for 5 minutes). The maximum of the mean curve (calculated from the ascending and the descending curve) was selected as stimulus intensity for further experiments. This procedure was followed by five sessions of 20 minutes mfb self-stimulation. Here, mice had to perform with an average frequency of at least 1 lever press per second to be included in the present study. The average lever press rates were measured during these five sessions. For logistical reasons we did not determine the lever press rates in the SPECT-lab.

Self-stimulation mediated by optogenetic stimulation of the VTA

Mice in the optical stimulation group were injected with rAAV2/CamKIIa-hChR2(H134R)-eYFP viral vector (350 nl, titer: 2*1E + 12 particles/ml) into the left ventral tegmental area (3.1 mm posterior and 0.5 mm lateral to Bregma, 4.3 mm ventral to the brain surface) through a pulled glass capillary. Immediately afterwards, a 200 μm optic fiber (Doric Lenses, NA 0.37) with magnetic connector was implanted 200 μm dorsal to the injection site and mounted to the skull using dental acrylic. After a two-week recovery and expression period, mice were placed into the self-stimulation chamber for 20 min per day over 6 days. Self-stimulation behavior was typically acquired spontaneously within the first two sessions. To confirm the appetitive nature of the optogenetic stimulation, the fourth training session was followed by 20 min extinction. During this phase, lever presses were counted but no light was given in response to any presses. Only animals that showed at least a threefold higher rate during regular training as compared to the extinction phase were selected for the study. Optical stimulation consisted of 150 ms pulses of blue light from a DPSS laser (CNI Lasers, 473 nm, 4 mW transmitted into the implanted fiber assembly). This light intensity will lead to an irradiance of 3 mW/mm^2 or larger within approximately 400 μm of the fiber tip (Yizhar et al., 2011). Assuming a minimal effective light intensity of 1 mW/mm^2 (Mattis et al., 2011) tissue at a maximal distance of up to 700 μm can be excited. The light was delivered through an optical fiber and a fiber optic rotating joint (Doric

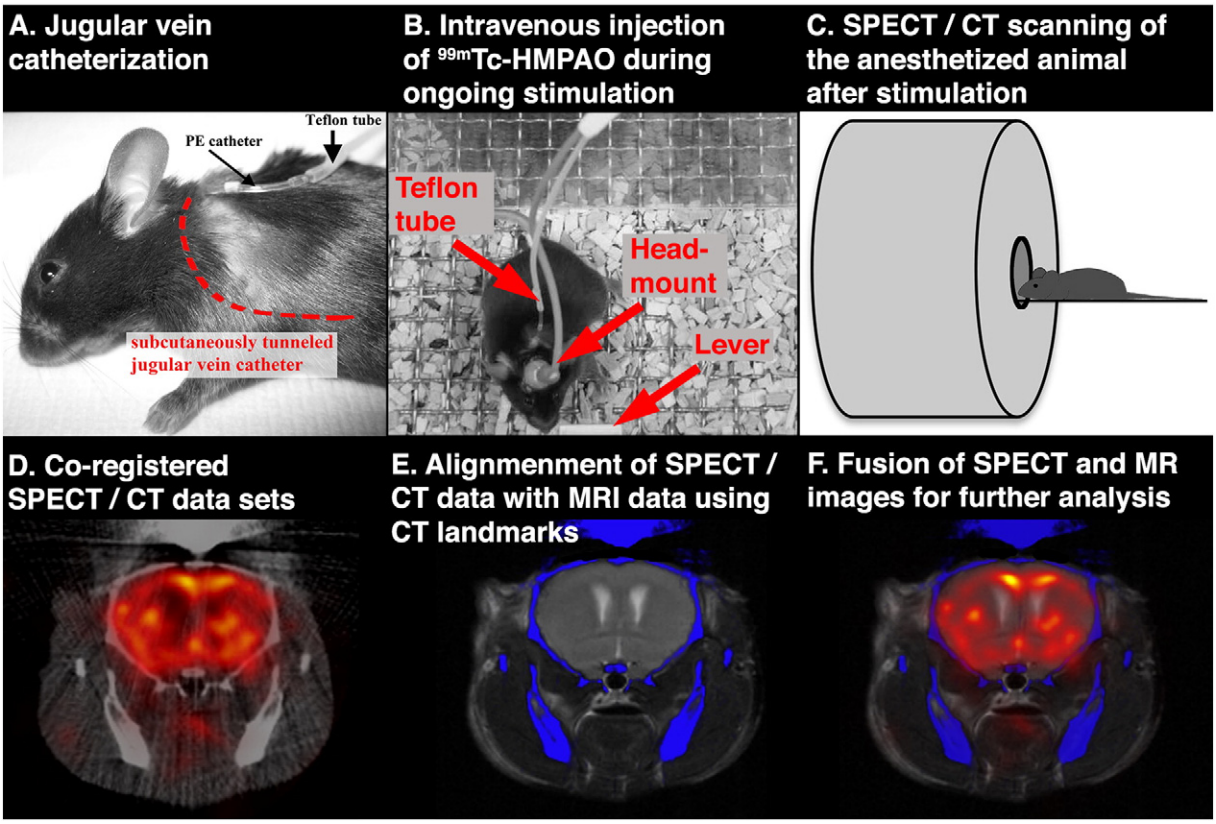

Fig. 1. Experimental procedure for SPECT-imaging of rCBF in intracranially self-stimulating mice. Mice were implanted with polyethylene catheters into the right external jugular vein two to three days before the first SPECT-imaging session. The catheters were subcutaneously tunneled. For intravenous injections of ^{99m}Tc-HMPAO the catheters were connected to a syringe via a teflon tube filled with saline. Mice were then transferred to the stimulation chamber. A photograph of the stimulation chamber is shown in B. The image is a view from above into the chamber showing a mouse with its head close to a lever. By lever-pressing mice could switch on either electrical currents or blue light for electrical or optical stimulation of the mfb or ChR2-expressing neurons in the VTA, respectively. The image shows the set-up for electrical stimulation. ^{99m}Tc-HMPAO was continuously injected during ongoing intracranial self-stimulation or control conditions without stimulation. Each animal was injected with ^{99m}Tc-HMPAO first under stimulus-conditions and two days later under control conditions. After each ^{99m}Tc-HMPAO injection mice were anesthetized and scanned. Co-registered SPECT/CT scans are made. Using CT-landmarks the SPECT/CT images were manually aligned with MR images. A SPECT/CT image is shown in D. (CT in gray scale, SPECT pseudocolored). A fused CT/MR image after alignment with MR data from the same individual is shown in E (CT blue, MR gray scale), a SPECT/CT/MR image in F (SPECT in colors from red to yellow, CT blue, MR gray scale).

Lenses), to minimize the movement restrictions imposed by the fiber-optic cable.

Jugular vein catheterization

After being trained for electrical or optogenetic self-stimulation, mice were implanted with a polyurethane catheter (ALZET, Cupertino, USA; 44.5 mm PU, OD: 0.84 mm, ID: 0.36 mm, connected to a 50 mm ALZET connection, OD: 1.02 mm OD, ID: 0.61 mm, total catheter length 9.5 cm) into the right external jugular vein under isoflurane anesthesia (1% isoflurane in 2:1 O_2:N_2O volume ratio) in the same manner as described previously for rodents (Goldschmidt et al., 2010; Lison et al., 2014). After implantation, animals were given at least two days to recover from surgery. Electrical or optogenetic self-stimulation was again confirmed in a single training session. For tracer injection, the catheter was connected to a teflon tube ("Tefzel-tube", CS-Chromatographie Service GmbH, D-52379 Langerwehe, Germany, OD: 1/16 inch ID: 0.5 mm) of 40 cm in length filled with 0.9% NaCl.

Preparation of ^{99m}Tc-HMPAO

The ^{99m}Tc-HMPAO injection solutions were prepared from commercially available kit preparations for clinical use (Ceretec^{TM}, GE Healthcare, Buchler, Braunschweig, Germany). The Ceretec^{TM} kit contains 0.5 mg exametazime (HMPAO) and 4.0 μg tin (II) chloride stored under nitrogen. In adult humans it is typically used for preparation of 750 MBq to 1 GBq ^{99m}Tc-HMPAO. In theory, this amount is sufficient for imaging about fifteen to twenty mice when doses of 50 MBq ^{99m}Tc-HMPAO per mouse are used as in the present study. In practice this is possible only, if the mice are either injected within a short time span of a few hours or if ways could be found to store aliquots of the kit. We found that efficient preparation of ^{99m}Tc-HMPAO was not possible after storing aliquots of the kit either dried or frozen in aqueous solutions. In half of the probes tested ($n = 14$) radiochemical purity was low ranging from 34% to 64%.

^{99m}Tc-HMPAO is synthesized by adding $^{99m}TcO_4^-$, the chemically stable ^{99m}Tc-compound delivered from ^{99m}Tc-generators, to HMPAO in the presence of a suitable reducing agent. The reducing agent in the Ceretec^{TM} kit is Sn^{++}. Sn^{++} is very sensitive to oxidation on air or in aqueous solutions and will be lost in the kit upon vial opening and adding of saline. We did not systematically explore how different freezing and storage conditions might minimize the loss of Sn^{++}. We instead added freshly prepared $SnCl_2$-solutions to the aliquots immediately upon use. This approach makes it possible to flexibly adjust and store small amounts of the kit substantially reducing the costs for rodent imaging.

We prepared HMPAO-aliquots by adding 4 ml 0.9% NaCl solution to the Ceretec^{TM}-kit. After mixing, aliquots of 250 μl were stored frozen at −80 °C. We used aliquots stored for up to two months. 30 min before the experiments aliquots were thawed. Five to ten min before use the ^{99m}Tc-HMPAO solution was prepared by adding 50 MBq ^{99m}Tc-pertechnetate in volumes of 50 – 75 μl 0.9% NaCl to the HMPAO-

aliquots. 25 μl of a 200 μM $SnCl_2$ solution were added just after mixing the ^{99m}Tc-pertechnetate solution with the HMPAO-aliquots. The 200 μM $SnCl_2$-solution was prepared just before use by adding 50 mg $SnCl_2$ x $2H_2O$ (Sigma-Aldrich, purissimum grade) to 1 L double-distilled H_2O and stirring for 30 sec. Radiochemical purity was 85% (n = 14) as determined according to the kit manufacturer´s guidelines (iTLC/SG MEK strips, iTLC/SG saline strips, Whatman paper acetonitrile strips; iTLC/SG chromatography paper was obtained from Agilent technologies, Whatman paper Grade B-2 from Sigma-Aldrich).

Intravenous injection of ^{99m}Tc-HMPAO

A syringe containing the freshly prepared 50 MBq ^{99m}Tc-HMPAO-solution was connected to the teflon tube and placed in a syringe infusion pump (Harvard Instruments). Injections were made at flow rates of 50 μl per minute during periods of seven to ten minutes. After ^{99m}Tc-HMPAO injection the teflon tube and the catheter were cleared with 0.9% NaCl during ongoing behavior or stimulation, respectively. Stimulation continued for two minutes after catheter clearance. Animals were then briefly induced with 3% isoflurane and transferred to the SPECT/CT-scanner. The amounts of ^{99m}Tc remaining in the syringe and in the teflon tube were determined using a radionuclide calibrator (Aktivimeter Isomed 2010, Nuklear-Medizin-Technik Dresden GmbH, Germany). Due to the high lipophilicity substantial amounts of ^{99m}Tc-HMPAO can be lost in plastic materials. On average 19% of the dose remained within the syringes and 9% within the teflon tubes. The teflon tubes were chosen in order to reduce the loss of ^{99m}Tc-HMPAO, which is higher in polyethylene tubes. An additional amount, visible in the SPECT images, remained attached to the jugular vein catheter. As parts of the catheters were outside the field of view the amount of ^{99m}Tc remaining in the catheters could not be determined in the SPECT-data sets. Two days after the first experimental session under self-stimulation conditions, a baseline measurement under identical conditions but without electrical or light stimulation was performed, during which the animals were free to press the - then dysfunctional - stimulation lever.

SPECT/CT imaging

SPECT/CT imaging was performed with a four head NanoSPECT/CT™ scanner (Mediso/Hungary). Animals were scanned under gas anesthesia (1.0-1.5% isoflurane in 2:1 O_2:N_2O volume ratio). The head-mounts for electrical and optical stimulation were used for head fixation in the animal bed. CT and SPECT were co-registered. CT scans were made at 45 kVp, 1.77 μA, with 180 projections, 500 msec per projection and 96 μm isotropic spatial resolution, reconstructed with the manufacturer´s software (InVivoScope 1.43) at isotropic voxel-sizes of 100 μm. SPECT scans were made using ten-pinhole mouse brain apertures with 1.0 mm pinhole diameters. 24 projections were acquired during a scan time of 2 hours. Axial FOV was 20.9 mm. Photopeaks were set to the default values of the NanoSPECT/CT (140 keV +/− 5%). SPECT images were reconstructed using the manufacturer´s software (HiSPECT™, SCIVIS, Goettingen) at an isotropic voxel output size of 167 μm. The spatial resolution was determined by analysis of the modulation transfer functions from line profiles through the jugular vein catheter with a known inner diameter of 0.61 mm. The line profiles were measured in radial and tangential direction for 9 consecutive images of the catheter filled with residual activity of Tc-99 m-HMPAO. The catheter was positioned perpendicular to the imaging plane and the MTF were estimated for each line profile. In concordance to other imaging modalities an MTF of 10% was chosen to define the spatial resolution in the imaging plane. Spatial resolution was about 0.7 mm full-width at half-maximum (FWHM) matching those of a previous study with the same scanner-type and a whole body mouse 1 mm multipinhole aperture (Apostolova et al., 2012).

Magnetic resonance imaging

Several days after the last SPECT/CT measurements animals were deeply anesthetized with pentobarbital (50 mg/kg), the implants were carefully removed to avoid MR-artefacts and the mouse heads were imaged on a Bruker Biospec 47/20 scanner at 4.7 T (free bore of 20 cm) equipped with a BGA 09 (400 mT/m) gradient system. A 25-mm Litzcage small animal imaging system (DotyScientific Inc., Colombus, SC, USA) was used for RF excitation and signal reception. Anatomical T2-weighted image with coronal (12 slices), axial (30 slices) and sagittal (17 slices) orientations were measured using a RARE (rapid-acquisition relaxation-enhanced) imaging sequence (Hennig et al., 1986) with the following parameters: TR 5150 ms (axial), 4000 ms (sagittal, coronal); TE 15 ms; slice thickness 0.6 mm; distance between slices 0.0 mm; FOV 30 × 30 mm; matrix 256 × 256 (resulting in a nominal in-plane resolution of 117 μm); RARE factor 8; number of averages 8; total scan time 56 min.

Histology

Brains of mice used for electrical self-stimulation were removed after MR imaging and rapidly frozen. Mice used for optical self-stimulation were perfused transcardially with 4% paraformaldehyde in phosphate buffered saline immediately after MR imaging. The brains were removed and sectioned on a vibratome at slice thicknesses of 60 to 100 μm. After mounting, slices were embedded in Mowiol. Viral expression, electrode or optical fiber placements were confirmed microscopically.

Data analysis

In each group, mfb-microstim (n = 5) and vta-optostim (n = 5), the brain ^{99m}Tc-distributions were compared under stimulus versus no-stimulus conditions. In addition, the tracer distributions under stimulus versus no-stimulus conditions were analyzed in a combined group (mfb-microstim plus vta-optostim). The analysis focused on voxelwise statistics of the data after alignment to a reference MR-image. A volume-of-interest (VOI) based analysis was performed for a cubic VOI with 700 μm edge length centered under the stimulation electrodes or optic fibers, respectively.

Different software tools were used for data analysis. Precise manual alignment of SPECT/CT-images to MR-images was done using the MPI-Tool™ software (version 6.36, ATV, Advanced Tomo Vision, D-50169 Kerpen, Germany). For the VOI-analysis the Osirix™-DICOM viewer (32-bit version 3.7 and 64-bit version 5.7.1) and Microsoft Excel (Versions 12.0 and 14.1) were used. Voxelwise statistics were done with the MagnAn-software (version 2.4, BioCom GbR, D-90180 Uttenreuth, Germany) (Knabl et al., 2008; Hess et al., 2011).

Data sets from SPECT/CT measurements were aligned to a high-resolution MR-mouse brain data set downloaded from the web (Ma et al., 2005, 2008). This high-resolution MR data set is from a C57/Bl6 mouse brain measured, after paraformaldehyde perfusion, ex vivo at 17.6 T with 47 μm isotropic resolution. The alignments were based solely on the best fit of CT- and MR-images. The CTs were aligned to MR-images based on skull-landmarks. The coordinates of the aligned CTs were used for alignment of the co-registered SPECT-data. The coordinates of the SPECT data relative to the CT data from the same measurement were not changed.

In the mfb-microstim group the electrode on the right side was chosen for self-stimulation in four animals, the electrode on the left side in one animal. For the group analysis mirror images of the SPECT/CT data, stimulus and control, from the left-side stimulating animal were aligned to the MR images. For analysis of the data in the combined group (mfb-microstim plus vta-optostim) all SPECT/CT data from the vta-optostim group were mirror-imaged.

For illustration of average MR/CT alignments, group CTs were made by summing up individual CTs of all animals in one group. After alignment all data sets were saved as DICOM-files with CT dimensions of 100 μm isotropic voxel sizes.

SPECT-brain data were cut out of the SPECT-data in Osirix™ using a whole-brain VOI made from the template provided by Ma and colleagues (Ma et al., 2005, 2008). In the mfb-microstim group slight deformations of the skull were present in regions surrounding the head-mount. These regions were not included in the analysis. Brain-SPECT data were normalized with the MPI-Tool™ software by using global mean normalization. For illustration of the mean ^{99m}Tc-distributions under different conditions normalized brain SPECT-data of each individual in a group were added. In voxelwise analyses paired t-tests were made in the mfb-microstim and vta-optostim group using the MagnAn-software. An unpaired t-test was made when comparing animals in the combined group (mfb-microstim plus vta-optostim) under self-stimulation versus no-stimulation conditions. Following previous studies in small-animal radionuclide imaging (Endepols et al., 2010; Marx et al., 2012; Thanos et al., 2013; Wyckhuys et al., 2010) uncorrected p-values were used.

Illustrations of the results were made in Osirix™. For fusion of three different imaging modalities, MR, CT and SPECT, a dual modality fusion, MR and CT, was created first, to which, after saving as DICOM-RGB file, a third modality was added. Images in Osirix™ were exported as TIFF files and arranged in the figures using the Photoshop™ software (version CS6).

Results

Changes in rCBF upon electrical self-stimulation of the mfb

In each individual mouse increases in rCBF at the stimulation site under stimulus-condition as compared to control could readily be observed in SPECT/CT data sets (Fig. 2). The mean lever press rates were 121.2 per min (SEM 15.1). Mean normalized ^{99m}Tc-content below the stimulation electrode as calculated from the VOIs in the normalized SPECT-data of the five mice increased by 38.6% as compared to control conditions. Tracer uptake and mean lever press rates were correlated ($r = 0.63$), but with the sample size of $n = 5$ the correlation did not reach statistical threshold. Differences in ^{99m}Tc-content were likewise immediately evident at the tip of the electrode used for stimulation compared to the non-stimulating electrode in the same animal. Electrode positions varied between animals (Fig. 3) but in the group analysis, nevertheless, a significant increase ($p < 0.01$) in rCBF could be observed in the stimulated region with single peaks of $p < 0.001$ (Fig. 4). The activated area extendend caudally into the VTA and the supramammillary region. Activations at the same significance levels of $p < 0.01$, again with peaks of $p < 0.001$, could be found ipsilateral to the stimulation site in the accumbens nucleus (Fig. 4) and in a region medial to the mammilothalamic tract at the level of the zona incerta and ventromedial thalamus. Significant deactivations ($p < 0.01$) in stimulated versus control condition were found in contralateral lateral septal/stria terminalis regions, the contralateral amygdala centered on the basomedial and/or central nucleus (Fig. 4), a midline thalamic region corresponding to reuniens and/or centromedian nucleus, bilaterally in parts of the dorsal and in the intermediate hippocampus (Fig. 4), bilaterally in parts of the retrosplenial cortex, bilaterally centered on the lateral habenula, in the contralateral geniculate nucleus and superior colliculus (Fig. 4) and in the dorsal raphe region.

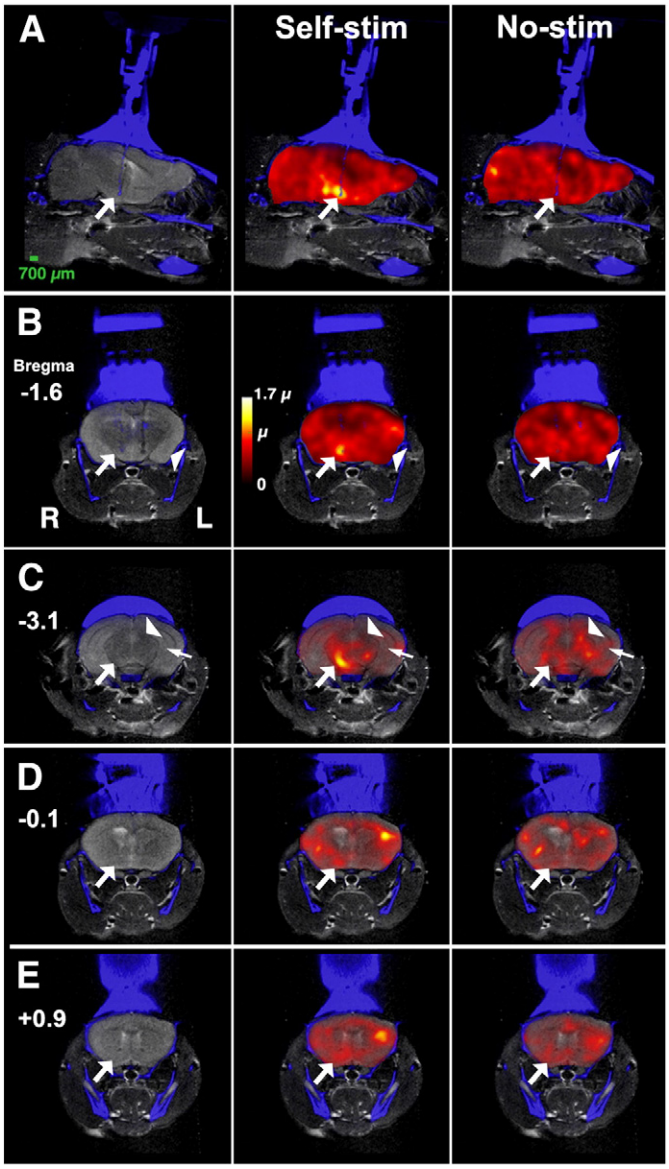

Fig. 2. Regional cerebral blood flow in an individual mouse during intracranial self-stimulation versus control condition without stimulation. In the column on the left CT images fused with MR images from the same animal are shown for illustrating anatomical relationships (MR grey scale, CT blue). In the other two columns SPECT-images of rCBF are overlaid on these MR/CTs. SPECT images in the middle column show rCBF under stimulus-conditions, SPECT images in the right column rCBF without stimulation. SPECT images are from global mean normalized brain-only data sets displayed on a logarithmic inverse scale ranging from 0 to 1.7 times the mean value (see scale in the middle panel of row B, μ = mean of all voxel values). SPECT-images in rows A and B are overlaid on MR/CT images with 100% opacity. Images in rows C, D and E are overlaid at reduced opacity in order to illustrate peaks in rCBF in relation to anatomical landmarks. The mouse had been implanted with one stimulation electrode on each side aimed at the left or right mfb, respectively. The electrode on the right side (R in B) was chosen for stimulation (arrows in rows A and B point to the electrode tip). Images in the sagittal plane are shown in A, in the frontal plane in B, C, D, E. Sagittal sections are 1 mm lateral from midline. Rostrocaudal coordinates of frontal sections relative to Bregma are given in the left column in B, C, D, E. Note focal increase in rCBF at the electrode tip. Note also that rCBF in the amygdala (arrowheads in B) on the left side under stimulus-condition is reduced compared to the control condition. RCBF is increased under stimulus-condition in the VTA, the medial forebrain bundle and the accumbens nucleus (arrows in C,D,E). RCBF under control condition is higher in the visual system (arrowhead at the superior colliculus in C) and in the contralateral intermediate hippocampus (small arrow in C).

Changes in rCBF upon optogenetic self-stimulation of the VTA

In optogenetically self-stimulating mice no significant changes in rCBF at the tip of the optic fibers were noted despite little inter-individual variance in fiber positions (Fig. 3). The mean lever press rates were 51.9/min (SEM 5.51). The VOI-based analysis revealed a statistically insignificant ($t = 1.46$) increase in normalized ^{99m}Tc-content of 3.6% under stimulus-conditions versus controls. ChR2-expression in the VTA was confirmed histologically in all animals. Significant increases ($p < 0.01$) in rCBF were found in close proximity to

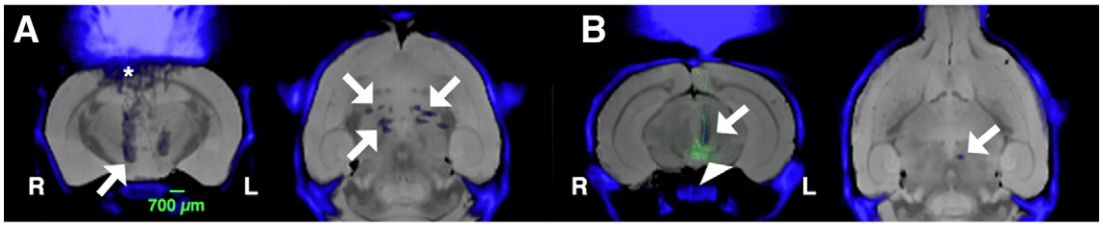

Fig. 3. Locations of stimulation electrodes and optic fibers. Shown are group CTs overlaid on MR images (CT blue, MR grey scale). CT images from the five individuals in each group were first aligned to a high-resolution ex vivo MR data set taken from Ma et al., 2005 and then added up to a single group CT. In the mfb-microstim group each of the five animals had been implanted with one electrode on the left and one electrode on the right side. The group CT thus contains five electrodes on each side. In the vta-optostim group each of the five animals had been implanted with a single optic fiber on the left side. The images show the group CTs overlaid on the reference MR in two orthogonal planes, a frontal plane and a horizontal plane at levels close to the tips of the electrodes or optic fibers, respectively. Images from the mfb-microstim group are shown in A, images from the vta-optostim group in B. The five electrodes on each side cluster rostrocaudally along the mfb (arrows in A). The five optic fibers are very closely aligned and merge into a single structure close to the VTA (arrows in B). A contrast enhanced image from a vibratome section from one individual with the eYFP fluorescence indicating ChR2 expression (arrowhead in B) is overlaid on the MR/CT. Note in A that the X-ray dense material overlying the cerebral cortex (asterisk) does not indicate cortical compression but is due to the overlay of the ten metal electrodes.

the stimulation site in the interpeduncular nucleus (Fig. 5). Typically, ChR2 expression extended into this nucleus (Fig. 3), but the calculated light intensity in this region was below 1 mW/mm^2, making it unlikely that action potentials could be elicited. Significant increases were also found in the lateral septum/bed nucleus of the stria terminalis region, in the accumbens shell (Fig. 5), in the contralateral dorsal tenia tecti region, bilaterally in motor and somatosensory cortices and in the ventromedial thalamus/medial zona incerta region. A prominent deactivation ($p < 0.01$) was found in the contralateral amygdala centered on the basomedial nucleus (Fig. 5). Deactivations upon stimulation were also found in the contralateral geniculate and substantia nigra.

Self-stimulation versus control in combined groups

Qualitative analysis of the data in each group, including differences in mean tracer uptake between stimulus and control conditions, suggested that the activation patterns with the different stimulation paradigms might be more similar than indicated by single probability maps at a certain threshold. For elucidating activation patterns common to both groups we pooled the data and tested all self-stimulating animals, mfb-microstim and vta-optostim, versus all controls. We detected a number of brain regions with highly significant activations and deactivations (Fig. 6). At $p < 0.01$ bilateral activations were found in orbitofrontal cortical regions, contralateral tenia tecti, ipsilateral activations in the rostromedial accumbens shell, in primary motor cortex, ventromedial thalamus/medial zona incerta, in the stimulated region comprising the ventral tegmental area, the supramammilary and the interpeduncular nucleus. In all regions small peaks were found with significance levels of $p < 0.001$. Deactivations were found on the contralateral side in the ventral pallidum, in the amygdala centered on the central and/or basomedial nucleus, the lateral habenula, the dorsal geniculate and superior colliculus, in the piriform cortex/amygdala region,

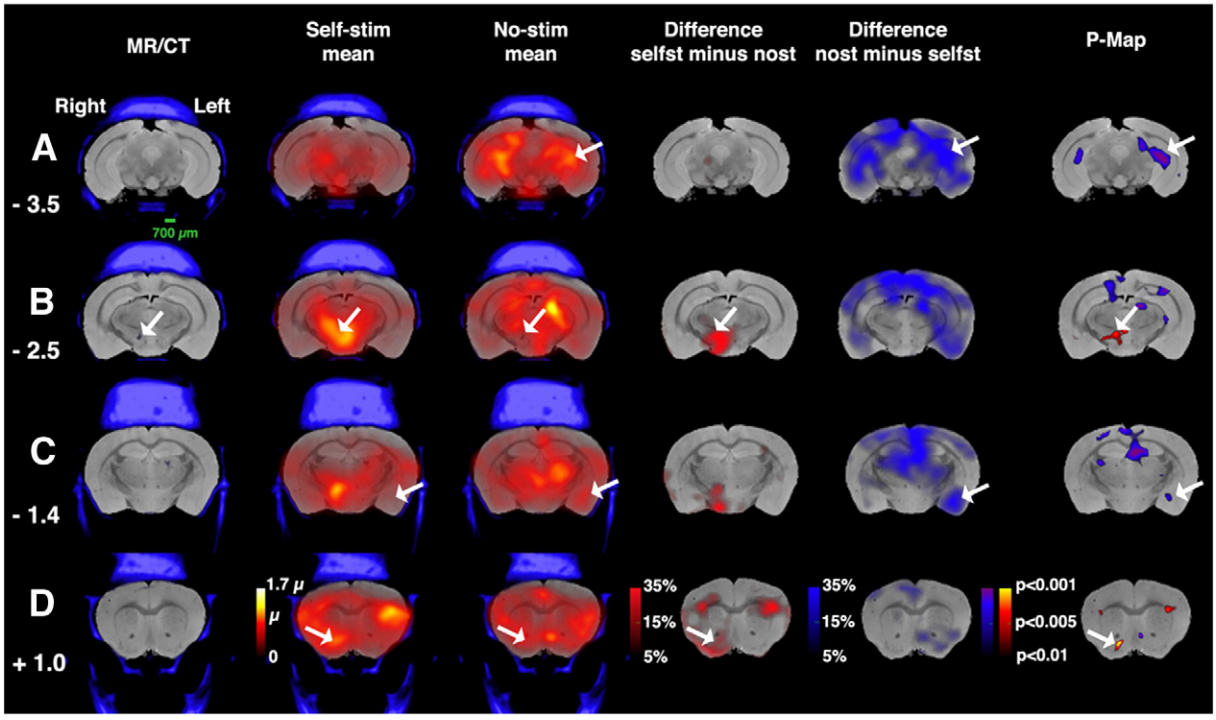

Fig. 4. Group data from mfb-microstim mice. Shown from left to right are group CTs overlaid on the reference MR for illustration of anatomical relationships and degree of MR/CT alignment, mean tracer uptake under self-stimulation condition and without stimulation, mean increases and decreases in tracer uptake under stimulus-condition versus control and probability maps. Of the five animals four were stimulated on the right side, one on the left side. The data from the left-side stimulated animal were mirror-imaged before being added to the other. Numbers on the left side from the MR/CTs indicate rostrocaudal coordinates relative to Bregma. Significant increases were found at the stimulation site (arrows in B) and the ipsilateral accumbens nucleus (arrows in D). Significant decreases were found bilaterally in the intermediate hippocampus (arrows in A), in the contralateral amygdala (arrows in C) and in the visual system (contralateral dorsal lateral geniculate and superior colliculus).

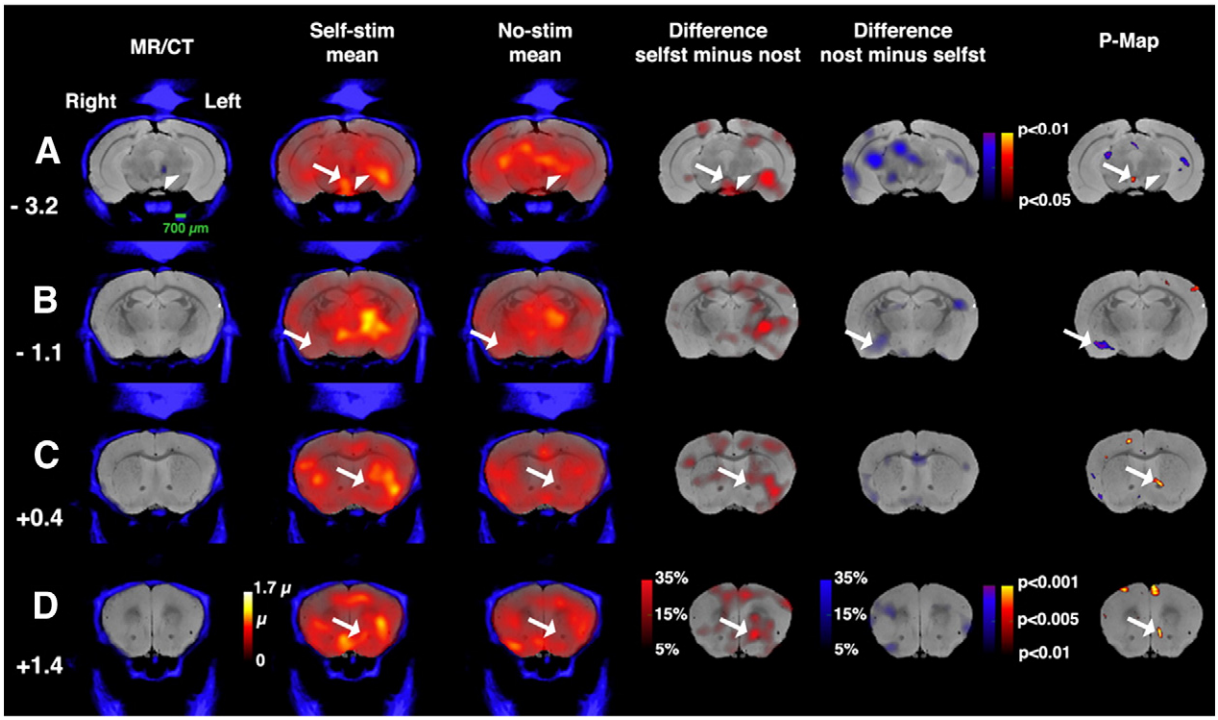

Fig. 5. Group data from vta-optostim mice. Same arrangement as in Fig. 4. All mice (n = 5) were stimulated on the left side. Significant increases in rCBF were found in the interpeduncular nucleus (arrows in A), in the area of the ipsilateral lateral septum/bed nucleus of the stria terminalis (arrows in C), ipsilateral nucleus accumbens (arrows in D) and in motor cortex. Decreases were found in the ipsilateral intermediate hippocampus, contralateral amygdala (arrows in B) and contralateral visual system. Note that the p-value scale in A is changed ($p < 0.05$). No significant changes were found at the tip of the optic fiber (arrowheads in A).

the lateral entorhinal cortex, bilaterally in the intermediate hippocampal formation, ipsilateral in the retrosplenial cortex and central gray and in a midline brainstem region corresponding to raphe nuclei. With the exception of the superior colliculus significance levels peaked in all these regions to levels of $p < 0.001$.

Discussion

^{99m}Tc-HMPAO SPECT imaging of rCBF in awake behaving mice

Two methods are currently in routine use for whole-brain in vivo imaging of spatial patterns of neuronal activity in awake behaving rodents, ^{18} F-FDG-PET (Kornblum et al., 2000) and manganese enhanced magnetic resonance imaging (MEMRI) (Silva et al., 2004). In the present study we have presented a novel approach. We intravenously injected awake behaving mice with the blood flow tracer ^{99m}Tc-HMPAO during several minutes of ongoing stimulation and mapped the brain tracer distribution using SPECT imaging.

The three different methods, MEMRI, ^{18} F-FDG-PET and ^{99m}Tc-HMPAO-SPECT, are similar in rationale. Animals are injected with tracers that accumulate in the brain in an activity-dependent manner during certain time spans of ongoing behavior. After accumulation the tracer distributions are determined in anesthetized animals.

Compared to MEMRI and ^{18} F-FDG-PET ^{99m}Tc-HMPAO-SPECT offers distinct advantages. MEMRI requires either invasive opening of the blood–brain barrier or stimulation times in the range of several hours (Silva et al., 2004). These stimulation times are unfavorably long for a large number of behavioral paradigms and, in addition, the images are influenced by axonal transport of manganese. Stimulation times in ^{18} F-FDG-PET are substantially shorter compared to MEMRI but the spatial resolution is lower than with small-animal SPECT, both with currently available systems as well as with respect to theoretical resolution limits.

Spatial resolution in PET imaging is limited by the positron range, i.e. the average distance between the positron-emitting atomic nucleus and the positron-electron annihilation site where the photons are generated that are finally detected. Theoretical resolution limits have been calculated (Rodríguez-Villafuerte et al., 2014) to be on the order of 500 µm when using the isotope ^{18} F, which has a comparably small positron range.

A fundamental resolution limit due to a mismatch between photon-emission sites and the positions of the radioactive atoms or labeled tracer molecules, respectively, does not exist in SPECT-imaging. Using pinhole imaging, which is based on the same geometric principle as the optical pinhole camera (Beekman and van der Have, 2007), spatial resolutions of 0.35 mm FWHM have been reported in the literature (van der Have et al., 2009), and mouse brain imaging at a resolution of 0.25 mm FWHM has been regarded as possible with current systems (van der Have et al., 2009). As with other imaging modalities there is a resolution-sensitivity trade-off, and with higher resolutions the applied doses and/or acquisition times will have to be increased. Protocols for ultra-high resolution small-animal SPECT-imaging of rCBF have not been developed thus far but, in principle, it seems possible to use ^{99m}Tc-HMPAO-SPECT for imaging rCBF at spatial resolutions with similar voxel sizes as in whole brain BOLD-fMRI imaging.

^{99m}Tc-HMPAO is a lipophilic compound that is rapidly cleared from the plasma (Andersen et al., 1988). Unlike ^{18} F-FDG or manganese (Mn^{++}), which can be intraperitoneally injected before stimulation, ^{99m}Tc-HMPAO has to be intravenously injected during ongoing stimulation in order to maintain flow-dependent wash-in of the tracer into the brain under stimulation-conditions. In anesthetized or restrained animals continuous intravenous injections can be made through the tail vein. In awake behaving animals stable chronic intravenous catheterizations are mandatory. We used jugular vein catheterization, a well-established approach routinely used in rodents for both chronic application of substances and blood sampling.

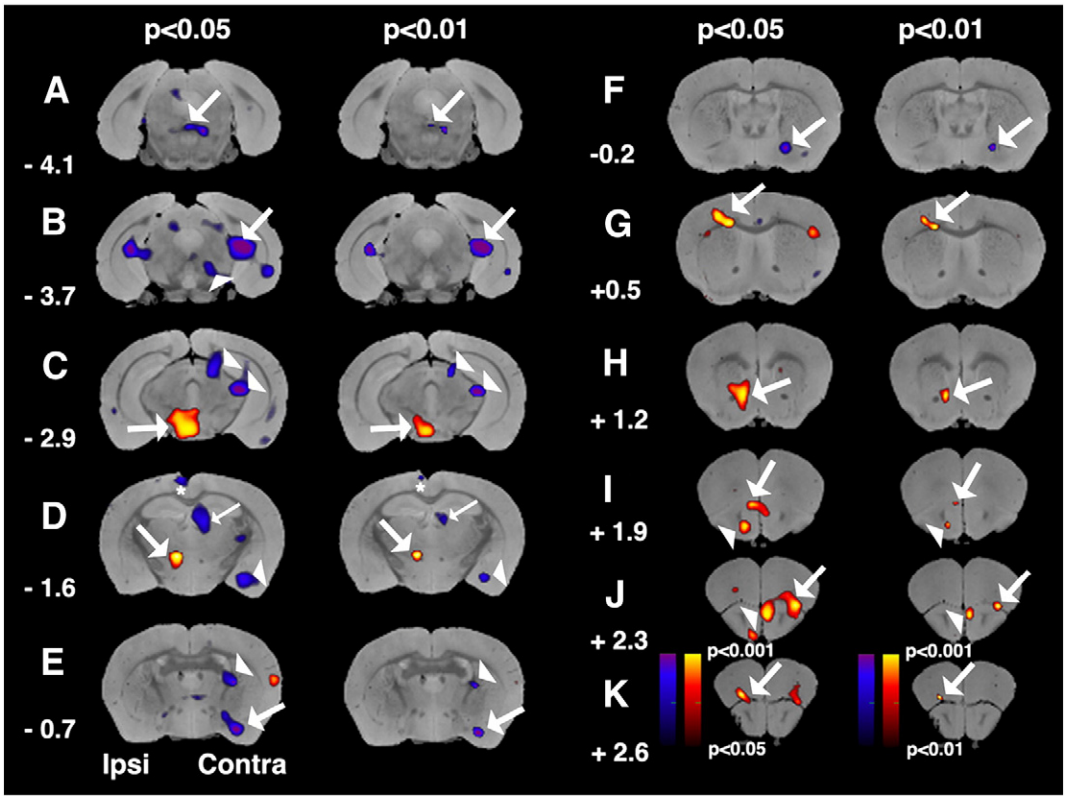

Fig. 6. Probability maps of pooled data from mfb-microstim and vta-optostim animals under stimulus-conditions versus control condition. Probability maps (P-Maps) are shown at two different significance levels in order to illustrate the different spatial extent of significant voxels above threshold. Sections are arranged from caudal (A) to rostral (K). Numbers on the left side of the sections indicate rostrocaudal coordinates relative to Bregma. For each section P-Maps at $p < 0.05$ are shown on the right, P-Maps at $p < 0.01$ on the left. Color look up tables for both maps are shown in K. Significant decreases in ^{99m}Tc-content under stimulus-conditions are color-coded from blue to violet, significant increases in red to yellow. Note decrease in the midline brainstem region corresponding to raphe nuclei (arrows in A), bilateral decrease in intermediate hippocampus (arrows in B), contralateral decrease in VTA/substantia nigra region (arrowhead in B), decrease in contralateral superior colliculus and dorsolateral geniculate nucleus (arrowheads in C), increase in ipsilateral VTA and supramammillary nucleus (arrow in C), increase in ipsilateral ventromedial thalamus/zona incerta region (large arrow in D), decrease in ipsilateral retrosplenial cortex (asterisk in D), contralateral epithalamus and adjacent regions (small arrow in D), decrease in contralateral amygdala (arrowheads in D and arrows in E), stria terminalis (arrowhead in E), contralateral ventral pallidum (arrow in F), increase in ipsilateral motor cortex (arrow in G), ipsilateral accumbens nucleus (arrow in H), contralateral tenia tecti (arrowhead in J) and adjacent midline cortical areas (arrow in I), ipsilateral anterior olfactory nucleus (arrowhead in I), and bilateral ventroorbital cortices (arrows in J and K).

The need for intravenous catheter implantation is certainly a drawback compared to MEMRI or ^{18}F-FDG-PET. On the other hand, the short plasma half-life of ^{99m}Tc-HMPAO makes short stimulation times possible. Brain uptake after intravenous ^{99m}Tc-HMPAO injections reaches a plateau within one minute after injection (Nakamura et al., 1989). In theory, using a single bolus-injection, the stimulation time could be similarly short. In practice, the minimum total stimulation time depends on the ^{99m}Tc-dose and the volume, respectively, that have to be injected to achieve sufficient signal-to-noise ratios at certain acquisition times and spatial resolutions. We injected 50 MBq ^{99m}Tc-HMPAO in ca. 500 μl saline at flow rates of 50 μl per minute and mapped the ^{99m}Tc-distribution at 0.7 mm FWHM isotropic resolution. This is a relatively low dose with ^{99m}Tc-HMPAO-concentrations in the injection solution similar to those used in human imaging. It seems possible to inject substantially higher doses at higher concentrations opening routes to higher spatial resolution, shorter acquisition times or shorter stimulation times. In addition, stimulus-triggered bolus-injections might be used to reduce the effective stimulation time to about one minute.

Activity-dependent changes in rCBF in electrically and optogenetically self-stimulating mice

We here present, to the best of our knowledge, the first in vivo imaging study of whole-brain activation patterns in intracranially self-stimulating mice. We co-registered rCBF SPECT scans with CT scans of 100 μm resolution. This enabled us to directly relate changes in rCBF to the position of the stimulation electrode or optic fiber, respectively, in each individual animal. In animals in which intracranial self-stimulation was mediated by electrical stimulation of the medial forebrain bundle we found strong increases in rCBF at the tip of the stimulation electrode. In contrast, with optical stimulation in mice expressing ChR2 in the VTA only a small statistically insignificant increase of 3.6% in ^{99m}Tc-content was present. We could rule out that this was due to ineffective ChR2-expressions or optic fiber misplacements. We calculated that with the light intensities we used the stimulation would be effective in an area up to about 0.7 mm around the tip, which in all animals well covered the VTA, and we histologically confirmed the eYFP expression after the final imaging session. Most importantly, the self-stimulation behavior per se indicates that the optical stimulation was effective.

This study was not designed to systematically explore differences in stimulation efficacy between electrical and optical stimulation. With different stimulation sites and protocols a number of effects may account for the observed phenomenon. Differences in lever press rates, differences in the density of excitable cells or fibers within a voxel, small spatial extent of excitation in case of optical stimulation resulting in partial volume effects, or excitatory and inhibitory feedback loops activated to different degrees in the different regions may all contribute to the effect. Alternatively or in addition, it could also be due to a more fundamental difference in the efficacy of both types of stimulation as shown recently in a study combining electrical and optical stimulation in macaque frontal eye field (Ohayon et al., 2013). In that study electrical stimulation was found to be more effective while optical

stimulation had similar effects to low-current electrical stimulation and did not result in a detectable fMRI signal at the stimulation site.

With both types of stimulation partially overlapping brain-wide networks of activations and deactivations were present. Upon optical stimulation of ChR2 expressing prinicipal neurons in the VTA we find areas of significant rCBF increases in the region of the lateral septum extending into the bed nucleus of the stria terminalis and in the nucleus accumbens shell. Activations in the accumbens shell were also found upon electrical stimulation of the medial forebrain bundle.

Similar to a recent ^{18} F-FDG-PET study (Thanos et al., 2013), where the effects of optogenetic stimulation of the nucleus accumbens were mapped in rat brain, we found deactivations in the default mode network in mfb-microstim mice. In that study an increase in glucose consumption in the contralateral amygdala was found upon stimulation. In our animals, in contrast, we found deactivations of the contralateral amygdala. It is noteworthy, however, that, besides differences in stimulation sites and protocols, the animals in our control condition were not naïve but pre-trained for self-stimulation. This pre-training might lead to shifts in baseline activity and up-regulation of the activity in the contralateral amygdala. Irrespective of the direction of changes both studies, ours and that of Thanos and colleagues (Thanos et al., 2013), indicate that effects on the contralateral amygdala may play an important role in the functional networks governing reward-mediated behavior upon unilateral stimulation.

When we pooled data from all animals, mfb-microstim plus vta-optostim, and tested self-stimulation versus control condition we found a network of activated and deactivated brain regions extending from the orbitofrontal cortices to the midbrain raphe region. Leaving open the question of potentially different contributions these regions might have in the different self-stimulation paradigms, we used the pooling of data as a heuristic approach for detecting regions involved in self-stimulation. In fact, most of the brain regions we found this way have been identified over the past decades as key structures of the reward circuitry in rodents and humans (Haber and Knutson, 2010; Ikemoto, 2010).

Highly significant increases in rCBF were present in the VTA and the accumbens shell nucleus. Interestingly, the location of significance peaks within the accumbens shell shifted from those in the individual groups to a region in the rostromedial shell that appears to very closely match with a homologous region described in rats as a “hedonic hotspot” in the accumbens shell (Berridge and Kringelbach, 2013). The activations in the VTA region extended into the supramammillary nucleus (SUM) supporting the view of cross-talks between VTA and SUM in the brain reward circuitry (Ikemoto, 2010; Ikemoto and Bonci, 2014). Besides activations in the reward circuitry we found increases in rCBF in motor cortex and related thalamic regions ipsilateral to the side of stimulation. It appears very likely that these activations reflect lever-pressing behavior and indicate that unilateral self-stimulation results in preferential use of ipsilateral forebrain motor systems. Conversely, deactivations were present in the visual system on the contralateral side indicating reduced input from or attention to the visual hemifield of the non-preferred side. The deactivations in the intermediate hippocampus, which were most pronounced on the contralateral side, might be directly related to this. Assuming reduced visuospatial processing under stimulus vs. control conditions and likewise reduced activity in subcortical limbic regions as the amygdala one might expect that the activity in the intermediate hippocampus, a region anatomically and functionally connected to both (Bast et al., 2009), decreases as well.

Our results clearly show that ^{99m}Tc-HMPAO SPECT is a powerful tool for imaging spatial patterns of neuronal activity in awake behaving mice.

^{99m}Tc-HMPAO SPECT as a novel tool for screening of regional brain activation patterns in awake behaving rodents

Wyckhuys and colleagues in a recent study in rats suggested the use of rCBF SPECT as a fast screening tool for evaluating stimulation paradigms and coil design in transcranial magnetic stimulation (Wyckhuys et al., 2013). With no need for cyclotron-produced short half-life radionuclides the logistics of SPECT-imaging are simpler than those of PET-imaging favoring more widespread uses of small-animal SPECT. The approach we have presented here substantially broadens the scope of potential applications of rCBF SPECT in rodents as it makes possible to study brain activation patterns in complex behavioral paradigms. In addition, our protocol of ^{99m}Tc-HMPAO synthesis from frozen aliquots of the commercial kit preparation markedly reduces the costs for SPECT-imaging of rCBF in the rodent brain. ^{99m}Tc-HMPAO SPECT could gain the same significance for imaging spatial patterns of neuronal activity in behaving rodents as BOLD-fMRI currently has for functional imaging in anesthetized or restrained rodents.

Acknowledgments

This work was supported by the German Federal Ministry of Education and Science (BMBF grants 01SF0718 and 03 V0765) and the Deutsche Forschungsgemeinschaft (SFB 779, SPP 1665). The authors wish to thank Ines Heinemann for excellent technical assistance and Karolin Gohlke for help with routine data processing.

Conflict of interest

The authors declare no competing financial interests.

References

Abe, Y., Sekino, M., Terazono, Y., Ohsaki, H., Fukazawa, Y., Sakai, S., Yawo, H., Hisatsune, T., 2012. Opto-fMRI analysis for exploring the neuronal connectivity of the hippocampal formation in rats. Neurosci. Res. 74, 248–255.

Andersen, A.R., Friberg, H., Knudsen, K.B., Barry, D.I., Paulson, O.B., Schmidt, J.F., Lassen, N.A., Neirinckx, R.D., 1988. Extraction of [99mTc]-d, l-HM-PAO across the blood–brain barrier. J. Cereb. Blood Flow Metab. 8, S44–S51.

Angenstein, F., Kammerer, E., Scheich, H., 2009. The BOLD response in the rat hippocampus depends rather on local processing of signals than on the input or output activity. A combined functional MRI and electrophysiological study. J. Neurosci. 29, 2428–2439.

Apostolova, I., Wunder, A., Dirnagl, U., Michel, R., Stemmer, N., Lukas, M., Derlin, T., Gregor-Mamoudou, B., Goldschmidt, J., Brenner, W., Buchert, R., 2012. Brain perfusion SPECT in the mouse: normal pattern according to gender and age. Neuroimage 63, 1807–1817.

Bast, T., Wilson, I.A., Witter, M.P., 2009. Morris RG (2009) From rapid place learning to behavioral performance: a key role for the intermediate hippocampus. PLoS Biol. 7 (4), e1000089 (Apr 21).

Beekman, F., van der Have, F., 2007. The pinhole: gateway to ultra-high-resolution three-dimensional radionuclide imaging. Eur. J. Nucl. Med. Mol. Imaging 34, 151–161.

Berridge, K.C., Kringelbach, M.L., 2013. Neuroscience of affect: brain mechanisms of pleasure and displeasure. Curr. Opin. Neurobiol. 23, 294–303.

Boyden, E.S., Zhang, F., Bamberg, E., Nagel, G., Deisseroth, K., 2005. Millisecond-timescale, genetically targeted optical control of neural activity. Nat. Neurosci. 8, 1263–1268.

Desai, M., Kahn, I., Knoblich, U., Bernstein, J., Atallah, H., Yang, A., Kopell, N., Buckner, R.L., Graybiel, A.M., Moore, C.I., Boyden, E.S., 2011. Mapping brain networks in awake mice using combined optical neural control and fMRI. J. Neurophysiol. 105, 1393–13405.

Endepols, H., Sommer, S., Backes, H., Wiedermann, D., Graf, R., Hauber, W., 2010. Effort-based decision making in the rat: an [18 F]fluorodeoxyglucose micro positron emission tomography study. J. Neurosci. 30, 9708–9714.

Goldschmidt, J., Wanger, T., Engelhorn, A., Friedrich, H., Happel, M., Ilango, A., Engelmann, M., Stuermer, I.W., Ohl, F.W., Scheich, H., 2010. High-resolution mapping of neuronal activity using the lipophilic thallium chelate complex TlDDC: protocol and validation of the method. Neuroimage 49, 303–315.

Haber, S.N., Knutson, B., 2010. The reward circuit: linking primate anatomy and human imaging. Neuropsychopharmacology 35, 4–26.

Hennig, J., Nauerth, A., Friedburg, H., 1986. RARE imaging: a fast imaging method for clinical MR. Magn. Reson. Med. 3, 823–833.

Hess, A., Axmann, R., Rech, J., Finzel, S., Heindl, C., Kreitz, S., Sergeeva, M., Saake, M., Garcia, M., Kollias, G., Straub, R.H., Sporns, O., Doerfler, A., Brune, K., Schett, G., 2011. Blockade of TNF-α rapidly inhibits pain responses in the central nervous system. Proc. Natl. Acad. Sci. U. S. A. 108, 3731–3736.

Ikemoto, S., 2010. Brain reward circuitry beyond the mesolimbic dopamine system: a neurobiological theory. Neurosci. Biobehav. Rev. 35, 129–150.

Ikemoto, S., Bonci, A., 2014. Neurocircuitry of drug reward. Neuropharmacology 76 (Pt B), 329–341 (Jan).

Kahn, I., Desai, M., Knoblich, U., Bernstein, J., Henninger, M., Graybiel, A.M., Boyden, E.S., Buckner, R.L., Moore, C.I., 2011. Characterization of the functional MRI response temporal linearity via optical control of neocortical pyramidal neurons. J. Neurosci. 31, 15086–15091.

Knabl, J., Witschi, R., Hösl, K., Reinold, H., Zeilhofer, U.B., Ahmadi, S., Brockhaus, J., Sergejeva, M., Hess, A., Brune, K., Fritschy, J.M., Rudolph, U., Möhler, H., Zeilhofer, H.U., 2008. Reversal of pathological pain through specific spinal GABAA receptor subtypes. Nature 451, 330–334.

Kornblum, H.I., Araujo, D.M., Annala, A.J., Tatsukawa, K.J., Phelps, M.E., Cherry, S.R., 2000. In vivo imaging of neuronal activation and plasticity in the rat brain by high resolution positron emission tomography (microPET). Nat. Biotechnol. 18, 655–660.

Lee, J.H., Durand, R., Gradinaru, V., Zhang, F., Goshen, I., Kim, D.S., Fenno, L.E., Ramakrishnan, C., Deisseroth, K., 2010. Global and local fMRI signals driven by neurons defined optogenetically by type and wiring. Nature 465, 788–792.

Lison, H., Happel, M.F., Schneider, F., Baldauf, K., Kerbstat, S., Seelbinder, B., Schneeberg, J., Zappe, M., Goldschmidt, J., Budinger, E., Schröder, U.H., Ohl, F.W., Schilling, S., Demuth, H.U., Scheich, H., Reymann, K.G., Rönicke, R., 2014. Disrupted cross-laminar cortical processing in β amyloid pathology precedes cell death. Neurobiol. Dis. 63, 62–67.

Ma, Y., Hof, P.R., Grant, S.C., Blackband, S.J., Bennett, R., Slatest, L., McGuigan, M.D., Benveniste, H., 2005. A three-dimensional digital atlas database of the adult C57BL/6 J mouse brain by magnetic resonance microscopy. Neuroscience 135 (4), 1203–1215.

Ma, Y., Smith, D., Hof, P.R., Foers ter, B., Hamilton, S., Blackband, S.J., Yu, M., Benveniste, H., 2008. In vivo 3D digital atlas database of the adult C57BL/6 J mouse brain by magnetic resonance microscopy. Front. Neuroanat. 2, 1. http://dx.doi.org/10.3389/neuro.05.001.2008.

Marx, C., Lex, B., Calaminus, C., Hauber, W., Backes, H., Neumaier, B., Mies, G., Graf, R., 2012. Endepols H (2012) Conflict Processing in the Rat Brain: Behavioral Analysis and Functional μPET Imaging Using [F]Fluorodeoxyglucose (2012). Front. Behav. Neurosci. 6, 4 (Feb 9).

Mattis, J., Tye, K.M., Ferenczi, E.A., Ramakrishnan, C., O'Shea, D.J., Prakash, R., Gunaydin, L.A., Hyun, M., Fenno, L.E., Gradinaru, V., Yizhar, O., Deisseroth, K., 2011. Principles for applying optogenetic tools derived from direct comparative analysis of microbial opsins. Nat. Methods 18, 159–172.

McArthur, C., Jampana, R., Patterson, J., Hadley, D., 2011. Applications of cerebral SPECT. Clin. Radiol. 66, 651–661.

Nakamura, K., Tukatani, Y., Kubo, A., Hashimoto, S., Terayama, Y., Amano, T., Goto, F., 1989. The behavior of 99mTc-hexamethylpropyleneamineoxime (99mTc-HMPAO) in blood and brain. Eur. J. Nucl. Med. 1989, 100–107.

Neirinckx, R.D., Canning, L.R., Piper, I.M., Nowotnik, D.P., Pickett, R.D., Holmes, R.A., Volkert, W.A., Forster, A.M., Weisner, P.S., Marriott, J.A., Chaplin, S.B., 1987. Technetium-99 m d, l-HM-PAO: a new radiopharmaceutical for SPECT imaging of regional cerebral blood perfusion. J. Nucl. Med. 28, 191–202.

Ohayon, S., Grimaldi, P., Schweers, N., Tsao, D.Y., 2013. Saccade modulation by optical and electrical stimulation in the macaque frontal eye field. J. Neurosci. 33, 16684–16697.

Paxinos, G., Franklin, K., 1997. The Mouse Brain in Stereotaxic Coordinates. Academic Press, San Diego (ISBN Number 0-12-26607-6; Library of Congress: QL937.F72).

Porrino, L.J., Esposito, R.U., Seeger, T.F., Crane, A.M., Pert, A., Sokoloff, L., 1984. Metabolic mapping of the brain during rewarding self-stimulation. Science 224, 306–309.

Rodríguez-Villafuerte, M., Yang, Y., Cherry, S.R., 2014. A Monte Carlo investigation of the spatial resolution performance of a small-animal PET scanner designed for mouse brain imaging studies. Phys. Med. 30, 76–85.

Silva, A.C., Lee, J.H., Aoki, I., Koretsky, A.P., 2004. Manganese-enhanced magnetic resonance imaging (MEMRI): methodological and practical considerations. NMR Biomed. 17, 532–543.

Thanos, P.K., Robison, L., Nestler, E.J., Kim, R., Michaelides, M., Lobo, M.K., Volkow, N.D., 2013. Mapping brain metabolic connectivity in awake rats with μPET and optogenetic stimulation. J. Neurosci. 33, 6343–6349.

van der Have, F., Vastenhouw, B., Ramakers, R.M., Branderhorst, W., Krah, J.O., Ji, C., Staelens, S.G., Beekman, F.J., 2009. U-SPECT-II: An Ultra-High-Resolution Device for Molecular Small-Animal Imaging. J. Nucl. Med. 50, 599–605.

Wyckhuys, T., Staelens, S., Van Nieuwenhuyse, B., Deleye, S., Hallez, H., Vonck, K., Raedt, R., Wadman, W., Boon, P., 2010. Hippocampal deep brain stimulation induces decreased rCBF in the hippocampal formation of the rat. Neuroimage 52, 55–61.

Wyckhuys, T., De Geeter, N., Crevecoeur, G., Stroobants, S., Staelens, S., 2013. Quantifying the effect of repetitive transcranial magnetic stimulation in the rat brain by μSPECT CBF scans. Brain Stimul. 6, 554–562.

Yizhar, O., Fenno, L.E., Davidson, T.J., Mogri, M., Deisseroth, K., 2011. Optogenetics in neural systems. Neuron 71, 9–34.